Construction and Building Materials 128 (2016) 38–46

Contents lists available at ScienceDirect

Construction and Building Materials

journal homepage: www.elsevier.com/locate/conbuildmat

# Expansion behavior of self-stressing concrete confined by glass–fiber composite meshes

Teng Man [a,b], Boxin Wang [a,*], Henan Jin [a,c], Xudong Zhang [a]

[a] College of Construction Engineering, Jilin University, 130021 Changchun, Jilin, China
[b] Department of Civil, Environmental, and Geo-Engineering, University of Minnesota, 55455 Minneapolis, MN, United States
[c] Changchun Institute of Optics, Fine Mechanics and Physics, Chinese Academy of Sciences, 130033 Changchun, Jilin, China

## HIGHLIGHTS

- Proposed that glass fiber composite meshes can be used as a reinforcement for SSC.
- Established the method for expansion strain calculation of CM-SSC.
- Analyzed the expansion behavior of SSC under restriction of composite meshes.
- Investigated the influence of mesh yarn and layer on expansion property of CM-SSC.

## ARTICLE INFO

*Article history:*
Received 4 April 2016
Received in revised form 15 September 2016
Accepted 6 October 2016
Available online 15 October 2016

*Keywords:*
Self-stressing
Expansion behavior
Composite mesh
Glass fiber

## ABSTRACT

Confined self-stressing concrete (SSC) efficiently improves the crack resistance of concrete materials. Considering the drawbacks of steel bar- or fiber-reinforced SSC, we propose glass–fiber composite mesh-reinforced SSC. Some mechanical properties of mesh-reinforced SSC have been investigated, but their expansion properties remain unclear. In this research, expansion experiments were conducted to understand the expansion behavior of this new combination. The development of expansion deformation was obtained and generalized using exponential and cotangential models. Theoretical analyses of the expansion behavior were deduced from the experimental results. The analyses showed that the expansion strain increases with the increment of width confinement and decreases with the increment of longitudinal confinement. Glass–fiber composite mesh-reinforced SSC has the potential to improve the crack resistance of concrete materials.



## 1. Introduction

Concrete, widely used as a structural material, can be applied to building engineering, transportation engineering, offshore platforms, and other engineering practices. However, concrete is brittle and has a small tensile strength. In addition, cement hydration is usually accompanied by volume shrinkage, which might lead to concrete cracks. Freeze–thaw effect, chloride or sulfur erosion, or other types of corrosions could dramatically decrease the strength and other properties of cracked concrete and harm the security of the entire structure [1,2]. Nowadays, concrete durability is important to the design of concrete structures.

Many types of special concrete, such as high-performance concrete, self-compact concrete, fiber-reinforced concrete, pre-stressed concrete, and carbon nanotube concrete, have been applied to engineering practices to enhance the durability of concrete materials [3,4]. However, such special types of concrete are usually expensive.

Self-stressing concrete (SSC) is a suitable crack-resistant material that can be easily applied in engineering practices [5]. The matrix in SSC can undergo large expansion deformation because of the chemical reaction inside the material [6]. Confinement of SSC by steel bars, steel fibers or textiles can introduce self-stresses that improve the crack resistance of the concrete matrix and the tensile strength of reinforced SSC members. In some cases, self-stress can even increase the compressive strength of the material to 8 MPa [7].

In the last 50 years, several studies have focused on self-stressing cement and expansion concrete in several countries. In particular, some studies have explored the expansion mechanism [8,9], pore property [10], and interfacial transition zone [11] of SSC. Other research has investigated the hydration process of

* Corresponding author.
*E-mail addresses:* manxx027@umn.edu (T. Man), boxinwang@jlu.edu.cn (B. Wang), jinhenanking@126.com (H. Jin).

http://dx.doi.org/10.1016/j.conbuildmat.2016.10.022
0950-0618/

expansion and self-stressing cement to identify the expansion components of expansive cement [12]. Experiments have also been conducted to understand the workability [13], mechanical properties, and durability of different types of self-stressing cement and concrete [14–16]. During hydration, AFt (abbreviation for "alumina, ferric oxide, tri-sulfate") can be produced from expansion components of self-stressing cement, which causes expansion deformation [17,18]. Volume expansion may dramatically decrease the strength of the interfacial transition zone and thus weaken the structure of SSC under unconfined conditions. By contrast, the microstructure of SSC can be greatly enhanced under confined conditions [19]. In most cases, SSC can be confined by steel bars, steel tubes, or short-cut fibers. Several studies have concentrated on steel bar-reinforced SSC, steel fiber-reinforced SSC, and steel tube filled with SSC. Calculation theories of self-stress of reinforced SSC were obtained. In general, the mechanical properties and durability of SSC specimens are better than those of normal concrete ones [20]. Among these studies, Jian-Guo Dai [14] presented a back-calculation method for predicting the deformation of self-stressing concrete based on BP-KX creep model, and proposed the calculation method for calculating the self-stresses of steel bar reinforced self-stressing concrete. Huanan He [21] and Boxin Wang [22] investigated the long-term expansive deformation of steel fiber reinforced self-stressing concrete and found out that the loss of self-stress is slight.

However, steel bar-reinforced SSC and other types of reinforced SSC also have inherent shortcomings. The steel bar used to reinforce SSC cannot influence the entire concrete cross-section uniformly. Placing the concrete near the steel bar could produce confinement, whereas placing the concrete far from the steel bar may cause deformation without confinement. Also, when the free expansion strain of the SSC matrix is too high, concrete located distant from the steel bar could incur cracks because of overexpansion. Meanwhile, the confinement efficiency in short-cut fiber-reinforced SSC is low because short-cut fibers are in 3D random distribution. The value and direction of self-stress in fiber-reinforced SSC are difficult to control [23].

SSC and glass–fiber composite mesh can be combined to realize a 2D confinement in SSC and thus allow the easy control of the value and direction of self-stress. A previous study [20] investigated the mechanical and bond properties of composite mesh-reinforced SSC (CM-SSC), but the expansion behavior of SSC under the confinement of composite meshes remains unclear. In this study, expansion experiments of both free SSC specimens and CM-SSC specimens were conducted. The general expansion scheme of both SSC and CM-SSC was obtained, and the influences of composite meshes on the expansion behavior of SSC were quantitatively investigated. Here we only investigate the specimens whose length is more than three times longer than its width. For specimens like this, the expansion in width direction can be neglected compare to the longitudinal expansion [6].

## 2. Materials and experiments

### 2.1. Experimental materials

Composite mesh-reinforced SSC consisting of self-stressing cement, coarse aggregates, fine aggregates, high-performance super-plasticizer, and glass–fiber composite meshes was used as the experimental object. Details about each material are enumerated below.

#### 2.1.1. Cement

Sulfur-type self-stressing cement (Chinese building industry standard JC715-1996) was used to obtain a large and stable expansion. The compressive strength of self-stressing cement is 43.8 MPa. The initial setting time is 70 min, and the ultimate setting time is approximately 99 min. Table 1 shows the detailed physical and chemical properties of this type of cement.

#### 2.1.2. Aggregates

River sand with a fineness modulus of 2.509 was used as fine aggregate, and limestone with a nominal diameter of 5–10 mm was used as coarse aggregate.

#### 2.1.3. Super-plasticizer

Concrete workability can be obtained by using the super-plasticizer. A high-performance poly-carboxylate super-plasticizer that meets the Chinese national standard GB 8076-2008 was applied. This high-performance super-plasticizer can be used in ready-mixed concrete, self-compact concrete, and high-performance concrete. No chloride ion and other erosion matters of concrete are included in this material.

#### 2.1.4. Mixture proportion of concrete

Concrete mixture should be designed specifically to obtain a suitable expansion capacity. The water/cement ratio was set to 0.36, whereas the cement/aggregate ratio was set to 0.50. The sand ratio was set to 45% on the basis of previous research [13,20]. Detailed mixture proportion is shown in Table 2. The amount of super-plasticizer added depended on concrete workability; thus, concrete slump tests were conducted. The slump value was approximately 53 mm when the contentment of super-plasticizer was 1.23 kg/m$^3$.

#### 2.1.5. Glass–fiber composite meshes

Alkali-resistant glass fiber roving that meets the Chinese building industry standard JC/T572-2002 was used in the glass–fiber composite mesh. The diameter of each filament is 13 μm, a single yarn consists of 9200 filaments, the linear density (the mass of textile per unit of length) of a single yarn is 2758 tex (tex means g/km), and the standard density (the mass of textile per unit of volume) of a single yarn is 2.77 g/cm$^3$. Thus, the whole cross-section area of a single yarn can be calculated as

$$A_y = \frac{m_y}{D_y}, \tag{1}$$

where $A_y$ is the cross-section area of a single yarn, $m_y$ is the linear density of a single yarn, and $D_y$ is the standard density of a single yarn. The cross-section area of a single yarn in this research was calculated to be approximately 0.996 mm. Glass–fiber composite meshes were fabricated by placing resin-penetrated yarns orthogonally. The mesh size was 40 mm × 40 mm. Concrete cannot penetrate into the yarn; thus, only outer filaments can develop a robust bond with the concrete matrix, which may considerably decrease the tensile capacity of the entire mesh cross-section. Hence, the fiber rovings were covered, penetrated, and fixed with epoxy resin to avoid tensile weakening and shear lag effect, as well as to bond two-way yarns. Figs. 1 and 2 show both unpenetrated and penetrated meshes, and Fig. 3 shows the microstructure of a penetrated yarn after fracture, in which we can see that the epoxy resin can penetrate the spaces between filaments.

### 2.2. Experimental works

Each specimen was 100 mm × 100 mm × 400 mm in size. Glass–fiber composite meshes were placed inside the concrete matrix symmetrically. The specimen was manufactured by placing a $H/(N+1)$-thick layer of SSC in the mold and positioning the mesh layer on top of this mold. $H$ is the height of the specimen, and $N$ is the total number of layers of glass–fiber meshes. Another $H/(N$

**Table 1**
Composition and properties of self-stressing sulfo-aluminate cement.

| Clinker: Dihydrate gypsum | Mineral composition (%) | | | Specific surface area ($cm^2/g$) | $SO_3$ (%) | Setting time (min) | | Compressive strength (MPa) |
|---|---|---|---|---|---|---|---|---|
| | $C_4A_2S$ | $\beta$—$C_2S$ | $CaSO_4 \cdot 2H_2O$ | | | Initial setting time | Ultimate setting time | |
| 71:29 | 48.26 | 19.36 | 26.60 | 4020 | 17.47 | 72 | 99 | 48.3 |

**Table 2**
Mixture proportion of self-stressing concrete ($kg/m^3$).

| Cement | Water | Coarse aggregate | Fine aggregate | Super-plasticizer |
|---|---|---|---|---|
| 686 | 247 | 754 | 617 | 1.23 |

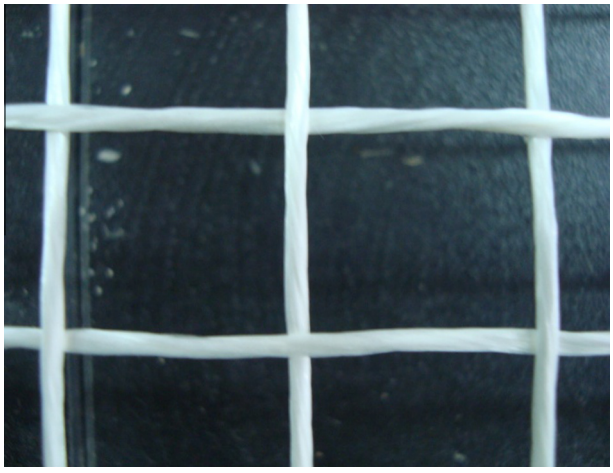

**Fig. 1.** Glass–fiber mesh before epoxy resin penetration.

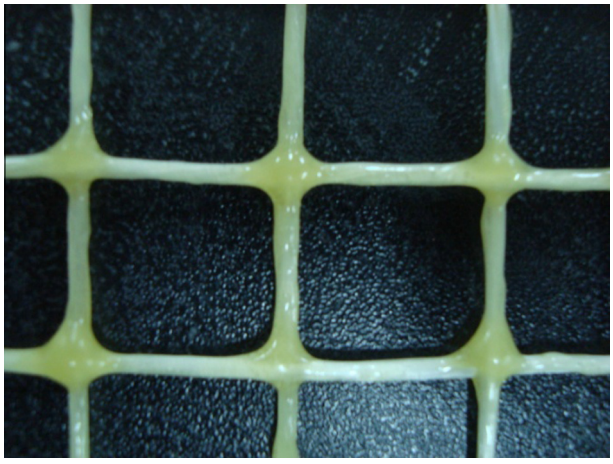

**Fig. 2.** Glass–fiber mesh after epoxy resin penetration.

+ 1)-thick layer of concrete was cast and slightly vibrated by a vibrator. Another mesh and concrete layer were placed, the mixture was vibrated, and the concrete mixture was positioned on top of the mold. In this research, the maximum and minimum numbers of mesh layers were 10 and 1, respectively. Specimens without composite meshes were also manufactured during the experiments. Each mesh layer has three longitudinal yarns and 10 lateral yarns. Each yarn can have several single yarns (each single yarn has a cross-section area of 0.996 $mm^2$). Table 3 shows the details of each specimen. Fig. 4 shows the manufacture scheme of

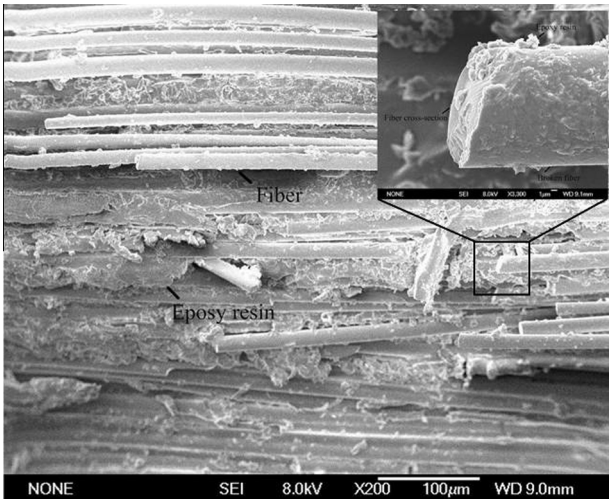


**Fig. 3.** SEM image of penetrated yarn after fracture.

SSC confined by glass–fiber composite meshes. Specimens were demolded after 24 h of curing in a standard curing box. The original length of each specimen was measured with a height caliper. In Table 3, SSC means self-stressing concrete, and CMSSC means composite mesh reinforced self-stressing concrete. Then, the three letters describe the longitudinal mesh ratio, width mesh ratio, and number of layer, respectively.

## 3. Results and discussion

### 3.1. Development of expansion deformation

SSC specimens with different confinement conditions display a similar process of expansion development. Considering that different specimens have different ultimate expansion strains, we used the normalization method to transform all of the experimental results to [0, 1] scale in accordance with the following equations:

$$\varepsilon_i = \frac{\Delta L_i}{L_0}, \varepsilon_{max} = \frac{\Delta L_{max}}{L_0} \quad (2)$$

$$\langle \varepsilon \rangle = \frac{\varepsilon_i}{\varepsilon_{max}} \quad (3)$$

where $\varepsilon_i$ is the longitudinal expansion strain after $i$ days of curing, $\Delta L_i$ is the longitudinal expansion deformation of a specimen after $i$ days of curing, $L_0$ is the original length of a specimen, $\Delta L_{max}$ is the maximum longitudinal expansion deformation of a specimen, $\varepsilon_{max}$ is the maximum longitudinal expansion strain of a specimen, and $\langle \varepsilon \rangle$ is the normalized longitudinal expansion strain.

**Table 3**
Details of specimens.

| Specimen No. | Volume ratio (Longitudinal) | Volume ratio (Width) | Layer number | Specimen No. | Fiber ratio (Longitudinal) | Fiber ratio (Width) | Layer Number |
|---|---|---|---|---|---|---|---|
| SSC | 0 | 0 | 0 | CMSSC-CED | 0.351% | 0.488% | 4 |
| CMSSC-AAD | 0.117% | 0.098% | 4 | CMSSC-DAD | 0.468% | 0.098% | 4 |
| CMSSC-ABD | 0.117% | 0.195% | 4 | CMSSC-DBD | 0.468% | 0.195% | 4 |
| CMSSC-ACD | 0.117% | 0.293% | 4 | CMSSC-DCD | 0.468% | 0.293% | 4 |
| CMSSC-ADD | 0.117% | 0.390% | 4 | CMSSC-DDD | 0.468% | 0.390% | 4 |
| CMSSC-AED | 0.117% | 0.488% | 4 | CMSSC-DED | 0.468% | 0.488% | 4 |
| CMSSC-BAD | 0.234% | 0.098% | 4 | CMSSC-EAD | 0.585% | 0.098% | 4 |
| CMSSC-BBD | 0.234% | 0.195% | 4 | CMSSC-EBD | 0.585% | 0.195% | 4 |
| CMSSC-BCD | 0.234% | 0.293% | 4 | CMSSC-ECD | 0.585% | 0.293% | 4 |
| CMSSC-BDD | 0.234% | 0.390% | 4 | CMSSC-EDD | 0.585% | 0.390% | 4 |
| CMSSC-BED | 0.234% | 0.488% | 4 | CMSSC-EED | 0.585% | 0.488% | 4 |
| CMSSC-CAD | 0.351% | 0.098% | 4 | CMSSC-GEA | 0.585% | 0.488% | 1 |
| CMSSC-CBD | 0.351% | 0.195% | 4 | CMSSC-FEB | 0.585% | 0.488% | 2 |
| CMSSC-CCD | 0.351% | 0.293% | 4 | CMSSC-DEE | 0.585% | 0.488% | 5 |
| CMSSC-CDD | 0.351% | 0.390% | 4 | CMSSC-BEF | 0.585% | 0.488% | 10 |

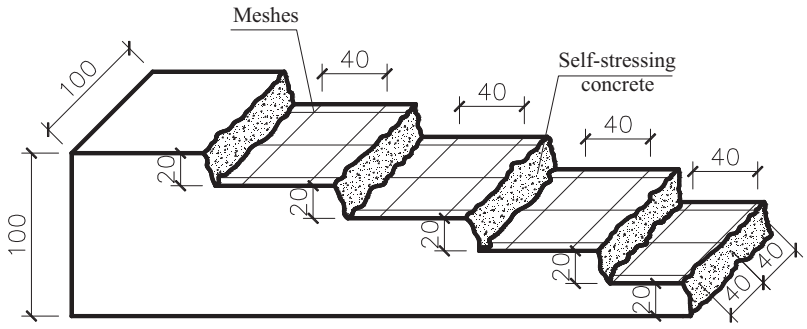


**Fig. 4.** Manufacture scheme of CM-SSC.

Fig. 5 shows the normalized experimental results, which are stable with a certain degree of discreteness. From Day 1 to Day 10, expansion deformations rapidly developed, whereas expansion deformations became stable after 10 days of curing. The development curve was described by an exponential function model or a cotangential function model. Both models were utilized to obtain easily the relative expansion strain. Then, the research point can focus on the ultimate expansion strain.

*3.1.1. Exponential function model*

Theoretically, when the curing time is $+\infty$, the derivative value is 0. Thus, the derivative function can be deduced as follows:

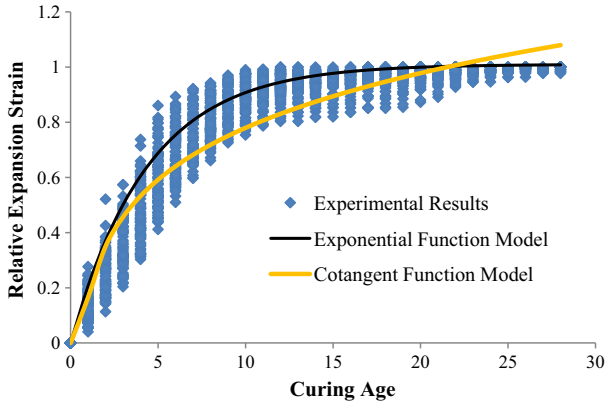


**Fig. 5.** Normalized longitudinal expansion strain and computational models.

$$\frac{d\langle\varepsilon\rangle}{dt} = \beta \exp(-\alpha t), \tag{4}$$

where $t$ is the curing time, and $\alpha$ and $\beta$ are constant values. Solving this differential equation, we can obtain the function of the normalized expansion strain as follows:

$$\langle\varepsilon\rangle = \gamma \exp(-\alpha t) + C, \tag{5}$$

$$\text{where } \gamma = -\frac{\beta}{\alpha} \tag{6}$$

On the basis of the regression analysis, $\gamma = -1.01$, $\alpha = 0.229$. The final results of the exponential function model are shown in Fig. 5. The R-square value of the exponential function model is approximately 0.836.

*3.1.2. Cotangential function model*

With the cotangential model, expansion development can be described as follows:

$$\langle\varepsilon\rangle = \cot(f(t)) = \frac{1}{\tan(f(t))} \tag{7}$$

Therefore,

$$f(t) = \arctan\left(\frac{1}{\langle\varepsilon\rangle}\right) \tag{8}$$

Regression analysis can be used to obtain the relationship between $f$(t) and $t$.

$$f(t) = 1.407t^{-0.19} \tag{9}$$

Therefore,

$$\langle\varepsilon\rangle = \cot(1.407t^{-0.19}) \tag{10}$$

Details about the expansion development of the cotangential model are shown in Fig. 5. The R-square value of the cotangential model is approximately 0.769.

### 3.2. Theoretical expansion analysis of CM-SSC

In traditional reinforced SSC, such as steel bar-reinforced and steel fiber-reinforced SSC, the steel bar or steel fiber serves as restrictions to establish self-stresses inside SSC. Similar to steel bars and steel fibers, glass–fiber composite meshes also serve as restrictions of SSC. In earlier research [19,20], a robust bond between the concrete matrix and meshes was established within the first 3 days of curing. The robust bond allows the meshes to deform with SSC. Meanwhile, SSC specimens with meshes show dramatically decreased expansion compared with non-restricted SSC specimens. The concrete matrix in steel bar-reinforced SSC is under unidirectional confinement, that in steel fiber-reinforced SSC is under 3D random restriction, and that in composite mesh-reinforced SSC is under bidirectional orthogonal restriction. The restriction in one direction largely influences that in the other direction.

In this research, we assumed that the principle of superposition holds for the entire analysis. In previous works [5,6,14], the expansion function of SSC under unidirectional confinement is expressed as follows:

$$\varepsilon_s = \varepsilon_f \exp(-\alpha\rho), \tag{11}$$

where $\varepsilon_s$ is the expansion strain under unidirectional confinement, $\varepsilon_f$ is the expansion strain without confinement (free expansion strain), $\alpha$ is the experimental constant, and $\rho$ is the confinement ratio of the cross-section. Thus, when confinement in the width direction exists, the expansion ratio in the width direction can be calculated using the following equation:

$$\varepsilon'_w = \varepsilon_w \exp(-\alpha_1\rho_w), \tag{12}$$

where $\varepsilon'_w$ is the expansion strain under width-direction confinement, $\varepsilon_w$ is the free expansion in the width direction, $\alpha_1$ is the experimental constant for width expansion, and $\rho_w$ is the confinement ratio in the width direction. Then, the difference between confined and free expansion strains can be calculated as follows:

$$\Delta\varepsilon_w = \varepsilon_w - \varepsilon'_w = \varepsilon_w[1 - \exp(-\alpha_1\rho_w)]. \tag{13}$$

Meanwhile, the restriction in the width direction can increase the expansion in the longitudinal direction. The increment of the longitudinal expansion strain due to width confinement can be calculated as follows:

$$\Delta\varepsilon_l = v\Delta\varepsilon_w = v\varepsilon_w[1 - \exp(-\alpha_1\rho_w)], \tag{14}$$

where $\Delta\varepsilon_l$ is the difference between the width-confined and free longitudinal expansion strains in the longitudinal direction, and $v$ is the deformation coefficient. Thus, the width-confined expansion strain in the longitudinal direction (in this case, we assume no longitudinal confinement exists) can be expressed as

$$\varepsilon'_l = \varepsilon_l + \Delta\varepsilon_l = \varepsilon_l + v\Delta\varepsilon_w = \varepsilon_l + v\varepsilon_w[1 - \exp(-\alpha_1\rho_w)], \tag{15}$$

where $\varepsilon_l$ is the longitudinal free expansion strain without both longitudinal and width confinements, and $\varepsilon'_l$ is the longitudinal free expansion strain with only width confinement. Adding a longitudinal confinement to the specimen alters the expansion strain on the basis of $\varepsilon'_l$ because of the previously assumed principle of superposition. Thus, the final longitudinal expansion strain with both longitudinal and width confinements can be calculated as

$$\begin{aligned}\varepsilon''_l &= \varepsilon'_l \exp(-\alpha_2\rho_l)\\ &= \{\varepsilon_l + v\varepsilon_w[1 - \exp(-\alpha_1\rho_w)]\}\exp(-\alpha_2\rho_l),\end{aligned} \tag{16}$$

where $\varepsilon''_l$ is the final longitudinal expansion strain, $\alpha_2$ is the experimental constant for longitudinal expansion, and $\rho_l$ is the confinement ratio for longitudinal direction.

However, the deformation change in the longitudinal direction can influence the expansion in the width direction, which finally influences the longitudinal expansion itself. Basing from the same analysis, we can calculate the longitudinal expansion change due to longitudinal confinement as follows:

$$\begin{aligned}\Delta\varepsilon_l = \varepsilon'_l - \varepsilon''_l &= \varepsilon'_l[1 - \exp(-\alpha_2\rho_l)]\\ &= \{\varepsilon_l + v\varepsilon_w[1 - \exp(-\alpha_1\rho_w)]\}[1 - \exp(-\alpha_2\rho_l)]\end{aligned} \tag{17}$$

This expansion change increases the expansion in the width direction by the following amount: $\Delta\varepsilon'_w = v\Delta\varepsilon_l$. However, this expansion change is influenced by width confinement. Thus, the width expansion decreases by the following amount:

$$\Delta\Delta\varepsilon_w = -v\Delta\varepsilon_l[1 - \exp(-\alpha_1\rho_w)]. \tag{18}$$

This decreased expansion increases the expansion in the longitudinal direction. The increment of longitudinal expansion can be calculated using the following equation:

$$\begin{aligned}\Delta\Delta\varepsilon_l &= v\Delta\Delta\varepsilon_w = v^2\Delta\varepsilon_l[1 - \exp(-\alpha_1\rho_w)]\\ &= v^2\{\varepsilon_l + v\varepsilon_w[1 - \exp(-\alpha_1\rho_w)]\}[1 - \exp(-\alpha_2\rho_l)][1 - \exp(-\alpha_1\rho_w)].\end{aligned} \tag{19}$$

This increment is also influenced by longitudinal confinement, which consequently yields the secondary increment in the longitudinal expansion strain:

$$\Delta\Delta\varepsilon'_l = \Delta\Delta\varepsilon_l \exp(-\alpha_2\rho_l) = v^2[1 - \exp(-\alpha_2\rho_l)]^2\varepsilon''_l, \tag{20}$$

where the deformation coefficient can be taken as Poisson's ratio of concrete material (usually 0.20). $[1 - \exp(-\alpha 1\rho h)]$ and $[1 - \exp(-\alpha_2\rho_z)]$ are both less than 1.0. Typically, $\exp(-\alpha_1\rho_h)$ and $\exp(-\alpha_2\rho_z)$ are both between 0.5 and 0.8. On the basis of the above assumptions, $\Delta\Delta\varepsilon'_z \leqslant 1\%\varepsilon''_z$, which makes $\Delta\Delta\varepsilon'_z$ negligible. Thus, the approximated final longitudinal expansion strain with both longitudinal and width confinements (in this case, mesh confinement) can be expressed as

$$\varepsilon''_l = \{\varepsilon_l + v\varepsilon_w[1 - \exp(-\alpha_1\rho_w)]\}\exp(-\alpha_2\rho_l), \tag{21}$$

where ν can be taken as Poisson's ratio (i.e., 0.20), and $\alpha_1$ and $\alpha_2$ are experimental constants that can be determined by the experimental data. In previous unidirectional confined expansion tests [6, 14, 22], $\alpha$ was always within the domain 200–300. Assuming that the SSC has the same property in every direction, we take $\alpha_1 = \alpha_2 = \alpha$. In this research, we set $\alpha$ to 205, which also fits the experimental results well.

### 3.3. Influence of composite meshes to SSC expansion

We present the experimental data and the theoretical solution together to analyze the influence of fiber yarns in both longitudinal and width directions on the longitudinal expansion behavior of specimens.

#### 3.3.1. Influence of longitudinal mesh yarn

Figs. 6–10 show the influence of fiber yarns in the longitudinal direction. Longitudinal yarns can dramatically decrease the expansion of SSC. These yarn directly cause self-stresses in the specimen body. The figures display that the theoretical fitting data can fit the experimental data well. The shape of the relationship curve between the yarn ratio and the experimental expansion strain is similar to the exponential function, which is also revealed in the analysis results. The experimental results are larger or smaller than theoretical results at some points. These errors are due to the

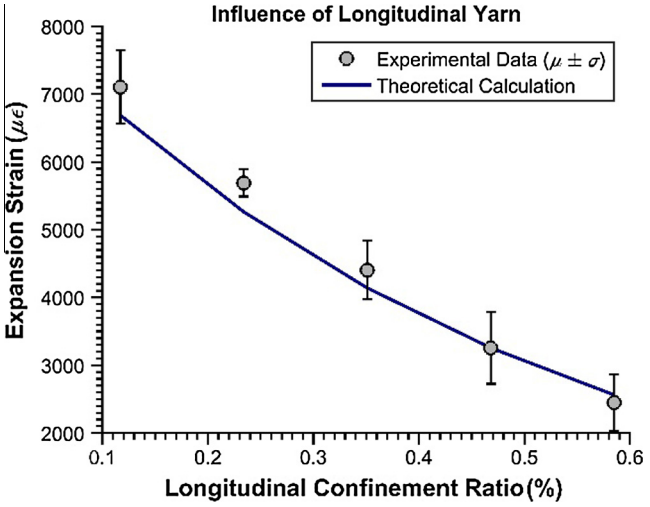


**Fig. 6.** Influence of longitudinal yarns when $\rho_w = 0.098\%$ (From left to right, the experimental data are collected from specimen CMSSC-AAD, ABD, ACD, ADD, AED, respectively).

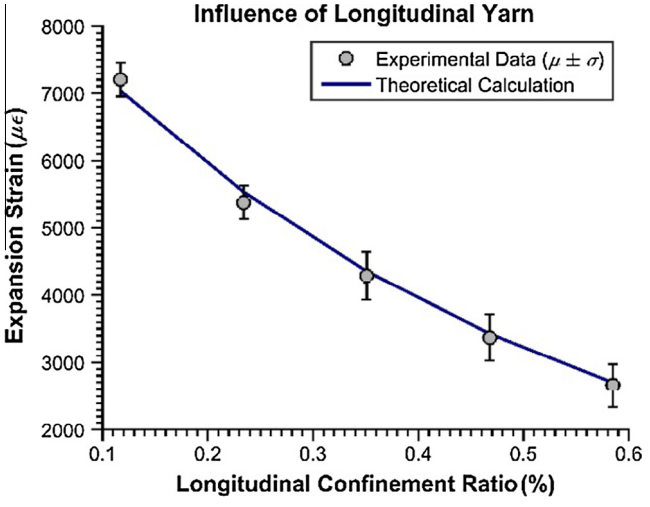


**Fig. 8.** Influence of longitudinal yarns when $\rho_w = 0.293\%$ (From left to right, the experimental data are collected from specimen CMSSC-CAD, CBD, CCD, CDD, CED, respectively).

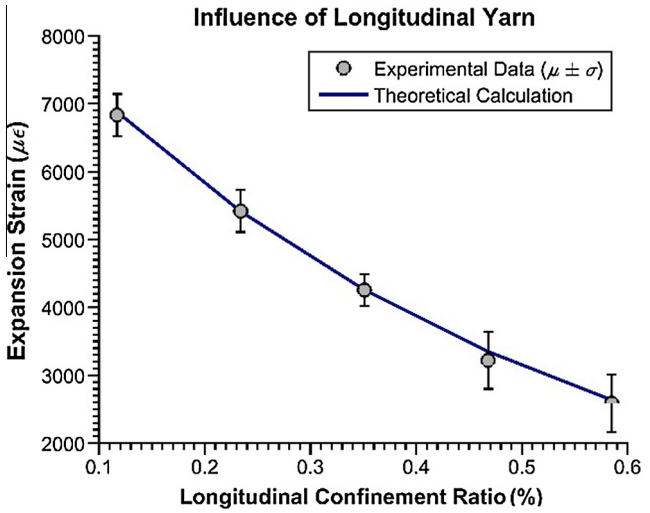


**Fig. 7.** Influence of longitudinal yarns when $\rho_w = 0.195\%$ (From left to right, the experimental data are collected from specimen CMSSC-BAD, BBD, BCD, BDD, BED, respectively).

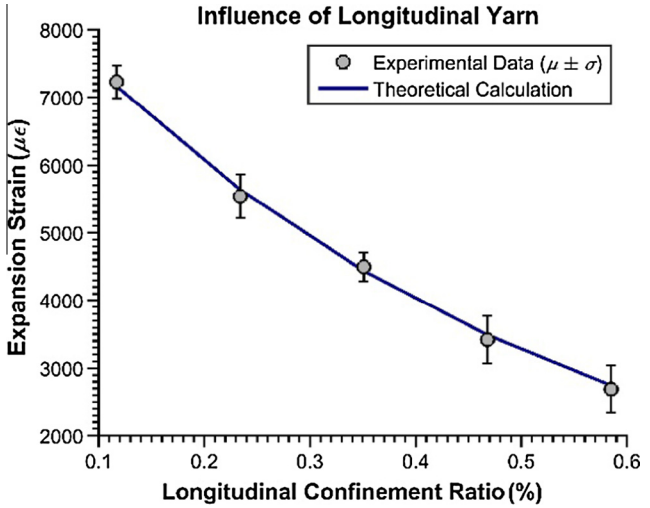


**Fig. 9.** Influence of longitudinal yarns when $\rho_w = 0.390\%$ (From left to right, the experimental data are collected from specimen CMSSC-DAD, DBD, DCD, DDD, DED, respectively).

manufacture of specimens. The meshes cannot be perfectly placed in the specimen as illustrated in Fig. 4.

### 3.3.2. Influence of width mesh yarns

Instead of decreasing the expansion of specimens, the width yarns can increase the expansion behavior. As shown in Figs. 11–15, the expansion strain of the specimens increases as the width yarn ratio increases from 0.098% to 0.488%. However, the experimental results of the specimens with $\rho_w = 0.098\%$ are much larger than the theoretical results when the longitudinal confinement is not strong enough. This result can be attributed to the fact that the expansion behavior becomes sensitive to the confinement in the width direction when the longitudinal yarn ratio is low, consequently increasing the expansion dramatically. However, the expansion decreases when the width yarn ratio gradually increases. After this small decline in expansion, the experimental data fit well with the theoretical prediction. This fitting proves to some extent that the experimental results are abnormal when $\rho_w = 0.098\%$. Generally, the transverse confinement can help increase the longitudinal expansion. However, it also depends on how well width (transverse) direction is confined. For small width confinement, the surface/volume ratio of textile mesh is actually higher, which can give us better mesh-concrete bond. So when width confinement is small, it can sometimes do a better job for confining concrete. The expansion sensitivity when the specimens are in a low confinement level may be due to the microscopic properties of the material, such as pore distribution and chemical reaction efficiency, which need to be investigated in the future.

### 3.3.3. Influence of the number of mesh layers

In this research, we are also interested in the influence of the spatial distribution of mesh layers. So we conducted several simple experiments for this topic. For the same confinement ratio of steel bar reinforced self-stressing concrete, the distribution of steel bars can greatly influence the expansion behavior of steel bar-reinforced SSC. Every confinement bar or fiber has an influential area within which the confinement is robust enough to prevent expansion. However, an unconfined area appears when the

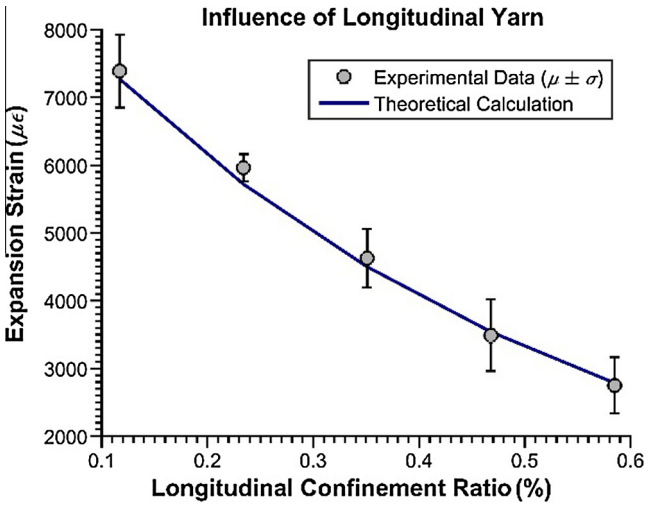


**Fig. 10.** Influence of longitudinal yarns when $\rho_w = 0.488\%$ (From left to right, the experimental data are collected from specimen CMSSC-EAD, EBD, ECD, EDD, EED, respectively).

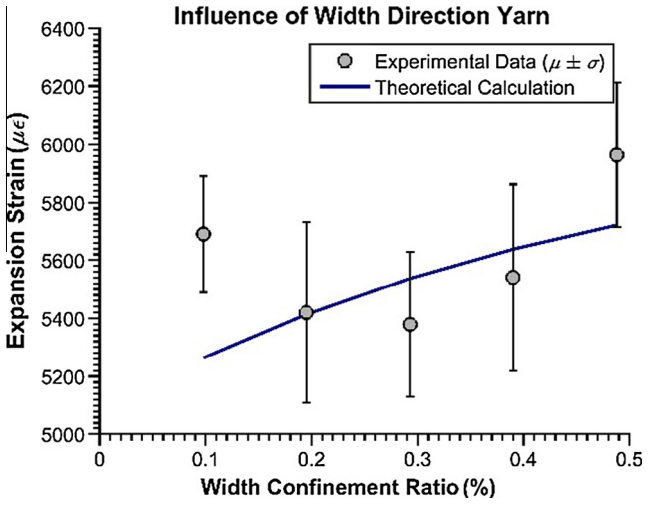


**Fig. 12.** Influence of width yarns when $\rho_l = 0.234\%$ (From left to right, the experimental data are collected from specimen CMSSC-ABD, BBD, CBD, DBD, EBD, respectively).

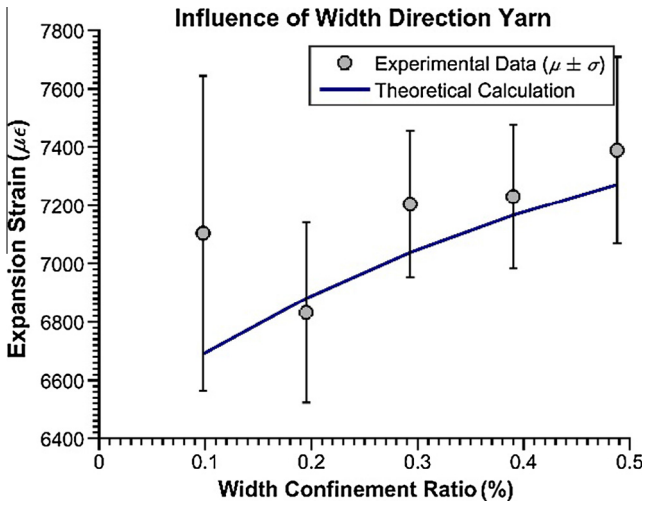


**Fig. 11.** Influence of width yarns when $\rho_l = 0.117\%$ (From left to right, the experimental data are collected from specimen CMSSC-AAD, BAD, CAD, DAD, EAD, respectively).

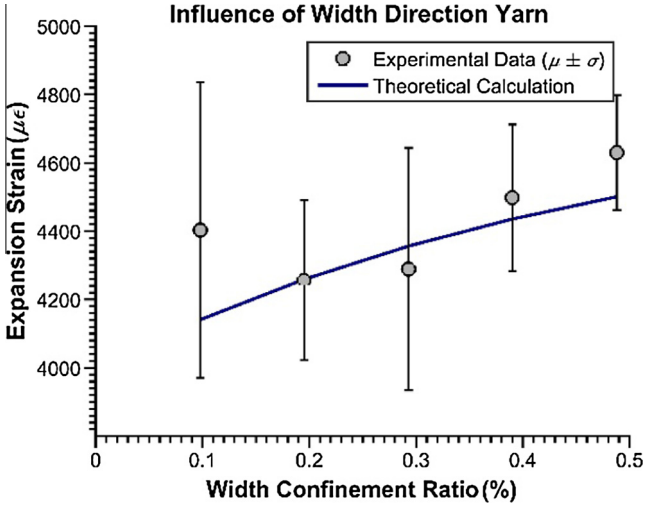


**Fig. 13.** Influence of width yarns when $\rho_l = 0.351\%$ (From left to right, the experimental data are collected from specimen CMSSC-ACD, BCD, CCD, DCD, ECD, respectively).

distance of the confinements is large enough, and the presence of this area decreases the confinement efficiency. Then, the experimental results might not be credible if the confinement is not efficient enough. The influence of layer number on expansion behavior must be investigated to ensure credible results. As shown in Fig. 16, increasing the layer number of meshes can greatly increase the confinement efficiency and decrease the expansion strain of the specimens when the confinement ratios of both longitudinal and width directions are remained constant at 0.585% and 0.488%, respectively. The layer numbers in the experiments were set to one, two, four, five, and ten. For a specimen with dimensions of $100 \times 100 \times 400$, 10 layers of meshes were used to ensure the robustness and efficient confinement of the specimens.

The experimental results in Fig. 16 show that the expansion strain is approximately 140% or 70% larger when the layer number is less than one or two than when it is ten. However, the expansion strain is approximately 25–30% larger when the layer number is four than when it is ten. Further increasing the layer number changes the confinement efficiency slowly. Considering both confinement efficiency and manufacture convenience, we deem that the results of the specimens with four mesh layers are not the best but still acceptable for further application. Basing from the experiments for specimens with different mesh layers, we can obtain the fitting function of this topic as follows:

$$\varepsilon_{exp} = 4976.8 \times N_{Layer}^{-0.373}, \tag{22}$$

where $\varepsilon_{exp}$ is the expansion strain, and $N_{Layer}$ is the number of mesh layers. The R-square number of this fitting function is 0.972. Obviously, increasing the layer number to more than ten does not mean a consistent increase in the expansion strain. In addition, the expansion strain reaches infinity when the number of mesh layers decreases to zero. When the mesh layer number is zero, the expansion strain becomes free. Thus, this fitting equation only holds for cases with layer numbers not greater than ten and not less than zero. However, this equation has no connection with previous theoretical equations. Details on this topic need to be investigated in the future.

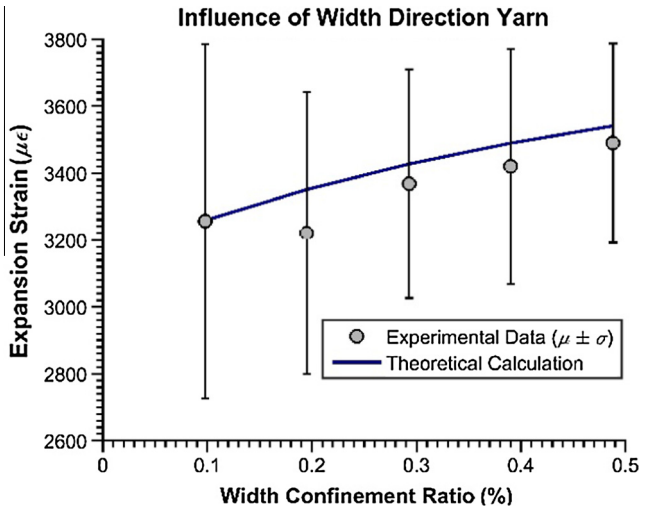


**Fig. 14.** Influence of width yarns when $\rho_l = 0.468\%$ (From left to right, the experimental data are collected from specimen CMSSC-ADD, BDD, CDD, DDD, EDD, respectively).

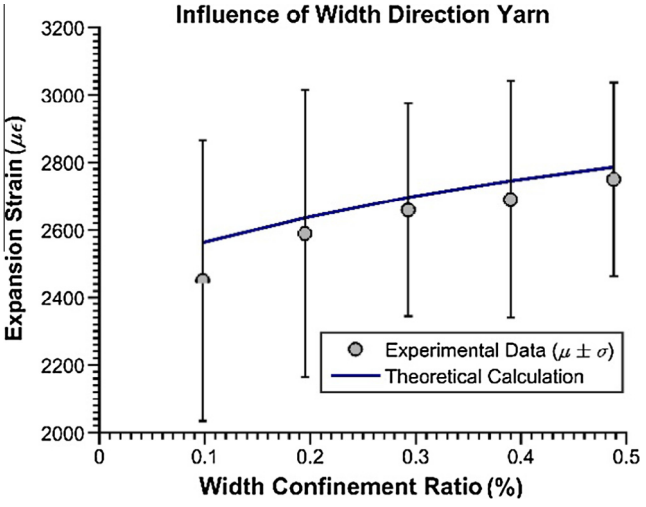


**Fig. 15.** Influence of width yarns when $\rho_l = 0.585\%$ (From left to right, the experimental data are collected from specimen CMSSC-AED, BED, CED, DED, EED, respectively).

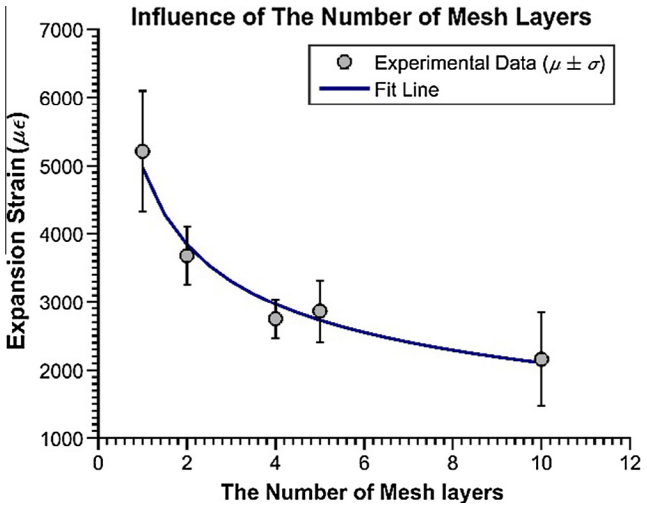


**Fig. 16.** Influence of the number of mesh layers (From left to right, the experimental data are collected from specimen CMSSC-GEA, FEB, EED, DEE, BEF, respectively).

## 4. Conclusions

In consideration of the several shortcomings of fiber- or steel bar-reinforced SSC, glass–fiber composite meshes were introduced to manufacture composite mesh-reinforced SSC. In general, glass–fiber composite meshes can be used as the confinement material for SSC. On the basis of both experimental works and theoretical analyses, conclusions can be summarized into the following:

(1) Experimental results of expansion within 28 days of curing were obtained, and a normalized form of expansion development was calculated from these results. Two fitting models, exponential and cotangential function models, were deduced from the normalized expansion strains. The normalized expansion strain was calculated using the two models. Further research can be focused on the properties and developing laws of the final expansion strain.

(2) In consideration of experimental data and previous research related to steel bar reinforced self-stressing concrete and steel fiber reinforced self-stressing concrete, theoretical analyses of the expansion behavior of SSC under the confinement of composite meshes were conducted on the basis of the assumption of superposition principle. The calculation equation of the expansion strain with respect to the longitudinal and width mesh ratios was deduced. The final equation shows that the relationship between the expansion strain and the confinement ratios is exponential type. This equation fits the experimental results very well.

(3) Based on the theoretical analysis, in the influence of longitudinal confinement ratio, width confinement ratio, and mesh layer number were investigated, respectively. The results show that the expansion strain increases with the increment of width confinement and decreases with the increment of longitudinal confinement. The existence of width confinement can largely improve the expansion property and increase the self-stress generated in the specimens. However, only a small fraction of confinement ratio and mesh layer number was investigated in this research. Thus, further experiments and analyses still need to be conducted in the future.

## Acknowledgements

Heartfelt thanks for the financial support of the China Postdoctoral Science Foundation (Grant No. 2015M581403), the National Natural Science Foundation of China (Grant No. 51108207), the Science and the State Key Program of Nation Natural Science Foundation of China (Grant No. 41430642). Teng Man also wants to thank Anu Tripathi for reviewing this paper and giving valuable suggestions.

## Appendix A. Supplementary data

Supplementary data associated with this article can be found, in the online version, at http://dx.doi.org/10.1016/j.conbuildmat.2016.10.022.

## References


[1] F.H. Wittmann, Crack formation and fracture energy of normal and high strength concrete, Sadhana 27 (4) (2002) 413–423, http://dx.doi.org/10.1007/BF02706991.

[2] C.Q. Li, S.T. Yang, Prediction of concrete crack width under combined reinforcement corrosion and applied load, J. Eng. Mech. 137 (11) (2011) 722–731, http://dx.doi.org/10.1061/(ASCE)EM.1943-7889.0000289.

[3] T.Y. Lim, P. Paramisivam, S.L. Lee, Bending behavior of steel-fiber concrete beams, ACI Struct. J. 84 (6) (1987), http://dx.doi.org/10.14359/2794.

[4] P.K. Mehta, P.J. Monteiro, Concrete: Structure, Properties and Materials, second ed., McGraw-Hill, New York, 1995. Unpublished manuscript for revision of Mehta, P.K and Monteiro, P.J.M. Concrete: Structure, Properties, and Materials.

[5] B. Wang, C. Huang, H. He, A study on the crack resistance of self-stressing concrete for old bridge rehabilitations, China Civ. Eng. J. 2 (2009) 86–91, http://dx.doi.org/10.7666/d.y714634 (in Chinese).

[6] J. Liu, Study on the deformation behavior, mechanical properties and microstructure of expansive concrete under different restraining conditions (Chinese Ph.D. dissertation), China Building Materials Academy, Beijing, China, 1991.

[7] W. Wang, J. Dai, Self-stressed steel fiber reinforced concrete as negative moment connection for strengthening of multi-span simply-supported girder bridges, Adv. Struct. Eng. 16 (6) (2013) 1113–1128, http://dx.doi.org/10.1260/1369-4332.16.6.1113.

[8] S. Nagataki, H. Gomi, Expansive admixtures (mainly ettringite), Cem. Concr. Compos. 20 (1998) 163–170, http://dx.doi.org/10.1016/S0958-9465(97)00064-4.

[9] E. Cecilie, S. Hansen, Expansive properties of ettringite in a mixture of calcium aluminate cement, Portland cement and b-calcium sulfate hemihydrate, Cem. Concr. Res. 31 (2001) 257–261, http://dx.doi.org/10.1016/S0008-8846(00)00495-6.

[10] L. Colin, M.D. Cohen, Pore structure development in type K expansive cement pastes, Cem. Concr. Res. 21 (1991) 229–241, http://dx.doi.org/10.1016/0008-8846(91)90003-Z.

[11] P.J.M. Monteiro, P.K. Mehta, The transition zone between aggregate and type K expansive cement, Cem. Concr. Res. 16 (1986) 111–114, http://dx.doi.org/10.1016/0008-8846(86)90075-X.

[12] L. Zheng, C. Xuehua, T. Mingshu, Hydration and setting time of MgO-type expansive cement, Cem. Concr. Res. 22 (1) (1992) 1–5, http://dx.doi.org/10.1016/0008-8846(92)90129-J.

[13] T. Man, B. Wang, H. Jin, Influence of sand ratio on the slump of self-stressingconcrete, Concrete 1 (2014) 98–101, http://dx.doi.org/10.3969/j.issn.1002-3550.2014.01.027 (in Chinese).

[14] J. Dai, C. Huang, Research on the basic mechanical properties of steel fiber reinforced self-stressing concrete, J. Build. Mater. 4 (1) (2001) 70–74, http://dx.doi.org/10.3969/j.issn.1007-9629.2001.01.014.

[15] Y. Wang, Y. Geng, G. Ranzi, et al., Time-dependent behaviour of expansive concrete-filled steel tubular columns, J. Constr. Steel Res. 67 (2011) 471–483, http://dx.doi.org/10.1016/j.jcsr.2010.09.007.

[16] C. Maltese, C. Pistolesi, A. Lolli, et al., Combined effect of expansive and shrinkage reducing admixtures to obtain stable and durable mortars, Cem. Concr. Res. 35 (12) (2005) 2244–2251, http://dx.doi.org/10.1016/j.cemconres.2004.11.021.

[17] M.S. Meddah, M. Suzuki, R. Sato, Influence of a combination of expansive and shrinkage-reducing admixture on autogenous deformation and self-stress of silica fume high-performance concrete, Constr. Build. Mater. 25 (1) (2011) 239–250, http://dx.doi.org/10.1016/j.conbuildmat.2010.06.033.

[18] H. Shuguang, L. Yue, Research on the hydration, hardening mechanism, and microstructure of high performance expansive concrete, Cem. Concr. Res. 29 (7) (1999) 1013–1017, http://dx.doi.org/10.1016/S0008-8846(99)00084-8.

[19] B. Wang, H. Jin, T. Man, et al., Study on the mechanical property of textile reinforced self-stressing concrete sheets, Constr. Build. Mater. 107 (2016) 1–10, http://dx.doi.org/10.1016/j.conbuildmat.2015.12.167.

[20] B. Wang, T. Man, H. Jin, Expansive and mechanical properties of textile reinforced self-stressing concrete, Constr. Build. Mater. 93 (2015) 1042–1050, http://dx.doi.org/10.1016/j.conbuildmat.2015.05.048.

[21] H. He, J. Qin, C. Huang, Research on long-term expansive deformation of steel fiber reinforced self-stressing concrete, J. Build. Mater. 12 (5) (2009) 595–598, http://dx.doi.org/10.3969/j.issn.1007-9629.2009.05.019.

[22] B. Wang, C. Huang, Study on long-term stability of self-stress create by steel fiber reinforced self-stressing concrete, J. North China Inst. Water Conserv. Hydroelectr. Power 33 (6) (2012) 86–88.

[23] H. He, C. Huang, Expansive characteristics and self-stress value of self-stressing concrete reinforced with steel bar and steel fiber, J. Build. Mater. 7 (2) (2004) 156–160, http://dx.doi.org/10.3969/j.issn.1007-9629.2004.02.006.